

Learning Prompt-Enhanced Context Features for Weakly-Supervised Video Anomaly Detection

Yujiang Pu¹, Xiaoyu Wu¹, and Shengjin Wang², *Senior Member, IEEE*

Abstract—Video anomaly detection under weak supervision is challenging due to the absence of frame-level annotations during the training phase. Previous work has employed graph convolution networks or self-attention mechanisms to model temporal relations, along with multiple instance learning (MIL)-based classification loss to learn discriminative features. However, most of them utilize multi-branches to capture local and global dependencies separately, leading to increased parameters and computational cost. Furthermore, the binarized constraint of the MIL-based loss only ensures coarse-grained interclass separability, ignoring fine-grained discriminability within anomalous classes. In this paper, we propose a weakly supervised anomaly detection framework that emphasizes efficient context modeling and enhanced semantic discriminability. To this end, we first construct a temporal context aggregation (TCA) module that captures complete contextual information by reusing similarity matrix and adaptive fusion. Additionally, we propose a prompt-enhanced learning (PEL) module that incorporates semantic priors into the model by utilizing knowledge-based prompts, aiming at enhancing the discriminative capacity of context features while ensuring separability between anomaly sub-classes. Furthermore, we introduce a score smoothing (SS) module in the testing phase to suppress individual bias and reduce false alarms. Extensive experiments demonstrate the effectiveness of various components of our method, which achieves competitive performance with fewer parameters and computational effort on three challenging benchmarks: the UCF-crime, XD-violence, and ShanghaiTech datasets. The detection accuracy of some anomaly sub-classes is also improved with a great margin.

Index Terms—Anomaly Detection, Context Aggregation, Prompt Learning, Weak Supervision.

I. INTRODUCTION

VIDEO anomaly detection (VAD) refers to the identification of uncommon events or behaviors that deviate from typical patterns in video streams [1]–[3]. Given the growing prevalence of surveillance cameras, human supervision alone is insufficient to fulfill the demands of practical applications. As such, the need for efficient and accurate automated VAD methods has rapidly increased in recent years. These methods have become increasingly important in various domains, including security and public safety, industrial process monitoring, healthcare, and social media analysis. By preventing potential threats and improving operational efficiency, VAD methods hold significant practical value.

In contrast to classical action recognition tasks, collecting relevant videos for anomaly detection poses a challenge due

to the sensitivity and scarcity of anomalous events. The mainstream approach treats anomaly detection as a semi-supervised learning task [4], wherein the characterization patterns of normal data are learned during the training phase, while identifying samples that deviate from the normality as anomalies [5]–[10]. While this paradigm does not necessitate fine-grained annotation, the non-exhaustive nature of normal patterns often results in the identification of unseen samples as anomalies, leading to a high false alarm rate.

In recent years, there has been a significant focus on developing more robust algorithms for anomaly detection, with particular attention given to weakly supervised approaches [11]–[15]. Compared to semi-supervised methods, weakly supervised paradigm offers several advantages: (1) The training data includes both normal and abnormal videos, enabling the model to learn more discriminative representations. (2) Weak supervision only requires video-level annotations, where the presence of anomalous events is indicated, but their start and end locations are unknown. (3) The absence of fine-grained annotations allows for the construction of large-scale datasets for anomaly detection. Thanks to these advantages, the weakly supervised approach has achieved superior performance and substantially outperforms the semi-supervised approach.

Considering that the duration of anomalous events can vary significantly, it is crucial to model the temporal relationship of video snippets to capture contextual information. Currently, graph convolutional networks [16] and self-attention mechanisms [17] are widely used for temporal relation modeling. However, the former only aggregates nodes within a finite neighborhood of video snippets, ignoring the integrity of anomalous events, while the latter primarily captures global correlations of all clips, which may introduce redundant noise. To address these limitations, Wu *et al.* [18] proposed an HL-Net with two paralleled graph convolutional networks to capture holistic and local dependencies, respectively, and obtained fused features through a simple concatenation operation. Similarly, Tian *et al.* [13] constructed an MTN network that combines multi-head self-attention and pyramid dilated convolutions to capture multi-scale temporal relations. These methods effectively consider local-global context modeling, thereby suppressing the interference of long-range noise. However, such parallel structure of multiple branches inevitably increases the parameters and computational cost, which may result in over-fitting.

In addition, the diversity and complexity of anomalies result in large intra-class variance and small inter-class variation within anomaly datasets, as depicted in Figure 1. Such datasets commonly include anomalous events in surveillance videos or

Corresponding author: Xiaoyu Wu.

Yujiang Pu and Xiaoyu Wu are with the School of Information and Communication Engineering, Communication University of China, Beijing 100024, China (e-mail: pyj2020@cuc.edu.cn; wuxiaoyu@cuc.edu.cn).

Shengjin Wang is with the Department of Electrical Engineering, Tsinghua University, Beijing 100084, China (e-mail: wsgj@tsinghua.edu.cn).



Fig. 1. Complex abnormal events from different acquisition sources. (a) UCF-Crime [11]. (b) XD-Violence [18].

in film and TV works. The former is captured by fixed-view cameras while the latter contains rich artistic expressions such as camera changes and scene switching. Building a robust anomaly detection pipeline in these complex scenarios is a challenging task. To address this issue, most studies construct a compact normal manifold with additional constraints. Wu *et al.* [12] introduced a center loss and a margin ranking loss to learn a discriminative decision boundary. Similarly, Park *et al.* [19] used learnable vectors to construct a set of prototypes for normal samples and introduced a normality-guided clustering loss with a triplet loss to enhance the inter-class separability between abnormal and normal snippets. However, these methods overlook the discriminability within anomaly classes, as illustrated in Figure 1, where there are significant differences between arson and fighting, burglary and shooting at the visual level, even though they are all anomalous events. Moreover, such binarized constraints fail to learn the specific semantics of anomalies, resulting in poor interpretability of predictions. Therefore, we contend that learning fine-grained context features for video anomaly detection is a critical aspect that facilitates the model to make more reliable decisions.

In this paper, we aim to address the two key issues mentioned above, i.e., temporal context modeling and limited anomaly discriminability, to further improve the anomaly detector. Firstly, we propose a temporal context aggregation (TCA) module to capture temporal relations across video snippets. Unlike existing parallel architectures in [13] [18] [20] [21], the TCA module enables efficient context modeling by reusing the similarity matrix. We also use a learnable factor for adaptive fusion of local-global contexts and embed a dynamic position encoding (DPE) into the similarity matrix, which uses a parametric kernel function to model the relative location of video snippets. Our TCA module outperforms existing

methods with fewer parameters and computational cost, as demonstrated by experimental results in Section IV.

Secondly, inspired by prompt learning [22], we propose a prompt-enhanced learning (PEL) module to strengthen the fine-grained semantics of context features, as shown in Figure 2. Existing methods [23]–[26] use hand-crafted or learnable vectors to construct prompt templates. The former are mostly class-agnostic phrases lacking sufficient context information, while the latter are abstract strings with weak interpretability. In contrast, we construct prompt templates by extracting relevant concepts from an external knowledge base, i.e., ConceptNet [27], which can serve as effective supplements to the context while possessing a certain degree of interpretability. By aligning anomalous contexts with their corresponding prompt features and repulsing non-anomalous contexts, rich semantics are injected into visual features to enhance their fine-grained discriminability. This operation also enlarges the inter-class separability between positive and negative snippets, which is conducive to forming a more discriminative decision boundary in the embedding space.

Finally, to address possible misclassifications caused by factors such as frame jitter or switching, we introduce a score smoothing (SS) module in the testing phase to suppress individual bias by applying average pooling to consecutive anomaly scores. This effectively improves the performance of our model while reducing false alarms in normal videos.

The main contributions of this paper are summarized as follows:

- 1) We construct a TCA module by reusing the similarity matrix and adaptive fusion for video anomaly detection, which achieves superior encoding performance with fewer parameters and computational cost.
- 2) We propose a PEL module that enables fine-grained context enhancement by constructing knowledge-based prompts, fore-background separation and cross-modal alignment.
- 3) Our model achieves competitive results on three benchmarks, i.e., UCF-Crime, XD-Violence, and ShanghaiTech dataset. We also observe a significant improvement in the detection accuracy of some fine-grained anomalies of approximately 10%.

The rest of the paper is organized as follows: Section II provides a review of the existing work on video anomaly detection and prompt learning. Section III presents the proposed method and its details. Section IV showcases the comparative results of state-of-the-art methods on three benchmarks and validates the effectiveness of each component through ablation studies. Finally, Section V concludes the paper.

II. RELATED WORK

A. Video Anomaly Detection

As previously noted, early work [28]–[31] considered anomaly detection as a semi-supervised learning task, i.e., only normal samples are available during the training phase, where statistical models with hand-crafted features were utilized. However, these approaches were limited by the weak representation ability of such features, leading to poor robustness and

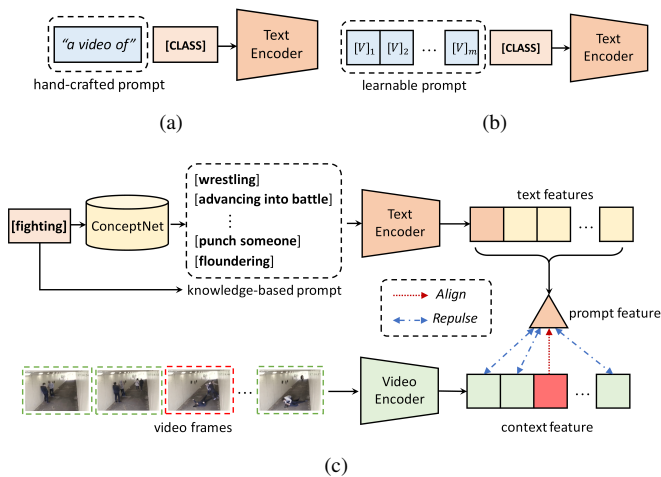


Fig. 2. Comparison of different methods for prompt construction. (a) Hand-crafted prompt. (b) Learnable prompt. (c) PEL module with knowledge-based prompt (Ours). The context features are enhanced by cross-modal alignment with the corresponding prompt features.

generalization. In recent years, the emergence of deep models has enabled the development of more powerful anomaly detection algorithms. Some approaches [32]–[35] aim to construct a one-class classifier that learns a compact manifold by constraining the latent space of normality, while identifying samples that deviate from that manifold as anomalies. However, due to the absence of a priori knowledge of anomalous events, some normal samples that are complex or unseen may be erroneously classified as anomalies. Other methods [36]–[38] assume that normality can be well reconstructed or predicted and identify samples with larger reconstruction or prediction errors as anomalies. Video anomaly detection commonly employs deep models such as U-Net [39], generative adversarial networks (GAN) [40], and ConvLSTM [41]. However, these methods are prone to over-fitting the training data, resulting in the reconstruction or prediction of some anomalies as normal events.

Recently, several studies have focused on weakly supervised anomaly detection, which involves training with both normal and abnormal samples that have video-level annotations. Sultani *et al.* [11] proposed a deep multi-instance learning model that utilizes a margin ranking loss to maximize the anomaly scores between positive and negative snippets. However, since the ranking loss requires paired inputs, Wan *et al.* [42] developed a dynamic multi-instance loss employing a top- k strategy. Subsequently, Tian *et al.* [13] introduced the Robust Temporal Feature Magnitude (RTFM) learning method to detect slight anomalies based on feature similarity and temporal continuity. The RTFM method parallelizes the self-attention block and pyramid dilated convolution layers to capture multi-scale temporal dependencies. Li *et al.* [43] proposed the Multi-Sequence Learning (MSL) method to refine localization boundaries by progressively optimizing a reduced sampled length. The self-attention mechanism incorporates Depth-wise Convolution to lower computational complexity for sequence correlation. Other studies, such as GCN-Cleaner [20] and MIST [44], generate high-confidence pseudo-labels

for video snippets, thereby transforming weakly supervised anomaly detection into a supervised learning task under noisy labels.

Although some of these approaches have investigated temporal relation modeling, many rely on parallel branches that require additional parameters and computations. In contrast, our method offers two distinct advantages. Firstly, the TCA module achieves local-global context encoding by reusing the similarity matrix, thereby outperforming methods that require extra branches in [13] [18] [21] [45] while using fewer parameters and computations. Secondly, our PEL module injects anomaly priors into the model through external knowledge instead of constructing the normality prototype from within the data as in [12] and [19]. This approach enhances the semantics of visual features and further improves the fine-grained anomaly detection performance of the model.

B. Prompt Learning in Video Understanding

Prompt Learning was originally proposed in the field of natural language processing with the goal of leveraging pre-trained models to achieve favorable generalization in few-shot or zero-shot scenarios via the design of suitable prompt templates. Recent research has successfully applied this approach to video understanding tasks. Wang *et al.* [24] aligned video clips with corresponding prompt embeddings of category labels for action recognition, incorporating category labels as prefix, fill-in-the-blank, and suffix into prompt templates to achieve superior performance over the single category prompt. Ju *et al.* [26] constructed prompt templates by combining category labels with a set of learnable vectors and explored the impact of label position in the templates. However, designing prompts manually is a time-consuming task and the model is sensitive to the content of the template [46]. While parametric prompts do not require linguistic priors, the learned prompts are often abstract strings with limited interpretability.

Yao *et al.* [47] utilized the definitions provided by WordNet [48] to create prompt templates. They also generated complementary descriptions of category labels by constructing a concept dictionary, which yielded outstanding results in open-vocabulary object detection tasks. Inspired by their work, we propose a novel prompt-enhanced learning approach for video anomaly detection. Our method differs from theirs in that we extract class-specific concepts highly relevant to anomalies from ConceptNet [27] to enrich potential context information. Furthermore, we aim to enhance the visual features by incorporating external prompts. To achieve this, we inject semantic information into visual features through cross-modal alignment, rather than bidirectional matching, which ensures that only visual features are required during the testing phase.

III. THE PROPOSED METHOD

In this section, we will introduce the proposed method for weakly-supervised video anomaly detection. Firstly, we present the overall framework, followed by a detailed elaboration of the core components.

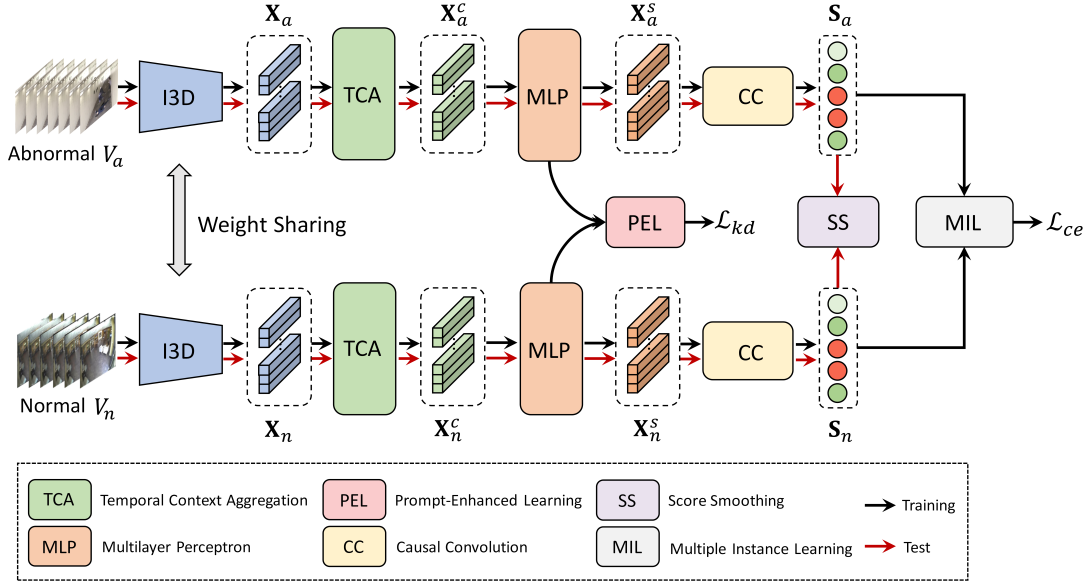


Fig. 3. Overview of our proposed framework. The model comprises six components in addition to the feature extraction network (I3D). The TCA module captures both local and global context simultaneously and facilitates adaptive fusion. The high-level representations are obtained using a two-layer MLP, with the PEL module operating in the middle layer to learn fine-grained semantics for context features. The CC module functions as a classifier to predict snippet-level anomaly scores. In the training phase, the model is optimized using both \mathcal{L}_{ce} and \mathcal{L}_{kd} , while SS is utilized for bias suppression during inference.

A. Overall Framework

The overall framework of our method is shown in Figure 3. Specifically, an untrimmed video is first divided into non-overlapping snippets by a sliding window of 16 frames. Subsequently, we use a pre-trained I3D network [49] to extract the snippet features \mathbf{X} , where the subscripts a and n denote abnormal and normal videos, respectively, which are fed into the TCA module to generate context features \mathbf{X}^c . After that, feature reduction is achieved through a two-layer multilayer perceptron (MLP), with the PEL module applied to the middle layer to learn discriminative features \mathbf{X}^s via knowledge-based prompts. Finally, the CC module predicts snippet-level anomaly scores \mathbf{S} . During the training phase, the MIL-based loss function converts the snippet-level scores into bag-level predictions to learn high activations for anomalous cases. In the testing phase, the SS module is utilized to suppress individual biases.

B. Temporal Context Aggregation Module

The TCA module aims to capture both global and local dependencies of snippets to model the complete temporal relationship, as shown in Figure 4. Following the self-attention mechanism [17], the snippet feature \mathbf{X} is first projected to the latent space by different linear layers, and the similarity matrix \mathbf{M} is obtained by computing the inner product as follows:

$$\mathbf{M} = f_q(\mathbf{X}) \cdot f_k(\mathbf{X})^\top, \quad (1)$$

$$\mathbf{A}^g = \text{softmax}\left(\frac{\mathbf{M}}{\sqrt{D_h}}\right), \quad (2)$$

$$\mathbf{X}^g = \mathbf{A}^g \cdot f_v(\mathbf{X}), \quad (3)$$

where $f_q(\cdot)$, $f_k(\cdot)$ and $f_v(\cdot)$ are three different linear mapping layers, \top refers to the transpose operation, and D_h is the

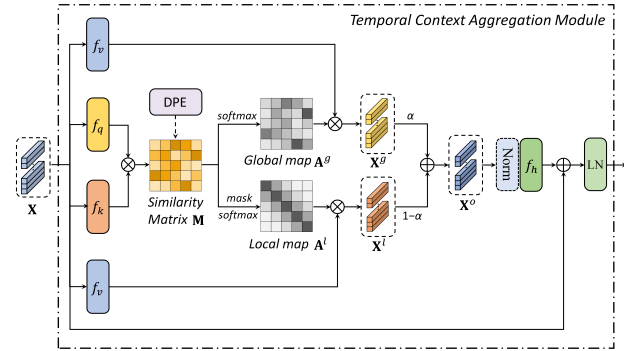


Fig. 4. Structure of the TCA module. DPE denotes dynamic position encoding.

hidden dimension in the latent space. Softmax normalization is then applied to generate the global attention map \mathbf{A}^g . The projected snippet feature is re-weighted by the attention map to obtain the global context feature \mathbf{X}^g .

Although the above operation facilitates global context modeling, it inevitably introduces long-range noise. To address this issue, we implement local context calibration by reusing the similarity matrix with a masking window. The process is denoted as:

$$\tilde{\mathbf{M}}_{ij} = \begin{cases} \mathbf{M}_{ij}, & \text{if } j \in [\max(0, i - \lfloor \frac{w}{2} \rfloor), \min(i + \lfloor \frac{w}{2} \rfloor, T)] \\ -\infty, & \text{otherwise} \end{cases} \quad (4)$$

$$\mathbf{A}^l = \text{softmax}\left(\frac{\tilde{\mathbf{M}}}{\sqrt{D_h}}\right), \quad (5)$$

$$\mathbf{X}^l = \mathbf{A}^l \cdot f_v(\mathbf{X}), \quad (6)$$

where w is the window size of the mask and T is the maximum length of the input sequence. Similarly, the projected snippet

feature is re-weighted with the attention map \mathbf{A}^l to obtain local calibration features \mathbf{X}^l , which can effectively capture slight changes and achieve feature enhancement in the local neighborhood.

Subsequently, a learnable weight is used to achieve local-global adaptive fusion, which is formulated as follows:

$$\mathbf{X}^o = \alpha \cdot \mathbf{X}^g + (1 - \alpha) \cdot \mathbf{X}^l, \quad (7)$$

$$\mathbf{X}^c = \text{LN}(\mathbf{X} + f_h(\text{Norm}(\mathbf{X}^o))), \quad (8)$$

where α and $1 - \alpha$ denote the global and local weight for context fusion, respectively, and $\text{Norm}(\cdot)$ denote a combination of power normalization [50] and L2 normalization. Then a linear layer $f_h(\cdot)$ followed by residual connection and layer normalization is applied to obtain context feature \mathbf{X}^c .

In addition, considering the importance of position information, we introduce Dynamic Position Encoding (DPE) to model the relative distances of snippets, formulated as:

$$\mathbf{G} = \exp(-|\gamma(i - j)^2 + \beta|), \quad (9)$$

where i and j denote the absolute positions of two snippets, and γ and β are learnable weights and bias terms. In particular, the DPE is embedded into the similarity matrix \mathbf{M} as a location prior, i.e., $\mathbf{M} \leftarrow \mathbf{M} + \mathbf{G}$, thus avoiding affecting the original feature distribution. Since DPE does not require a preset maximum sequence length, it is more flexible for variable-length videos. Also, it can suppress long-distance noises due to the properties of Gaussian-like kernel function.

C. Multilayer Perceptron and Causal Convolution

To obtain high-level semantic representations, a two-layer MLP is utilized for feature reduction, as shown in Figure 5. Each Conv1D layer is followed by a GELU activation and dropout operation. This process is denoted as follows:

$$\begin{aligned} \mathbf{X}^e &= \text{Dropout}(\text{GELU}(\text{Conv1D}(\mathbf{X}^c))), \\ \mathbf{X}^s &= \text{Dropout}(\text{GELU}(\text{Conv1D}(\mathbf{X}^e))). \end{aligned} \quad (10)$$

Finally, a causal convolution layer is employed to predict snippet-level anomaly scores, which considers both current and historical observations to obtain more reliable results. The classifier is formulated as:

$$\mathbf{S} = \sigma(f_t(\mathbf{X}^s)), \quad (11)$$

where $f_t(\cdot)$ is the causal convolution layer with kernel size Δt , $\sigma(\cdot)$ is the sigmoid function, and s_i is the anomaly score of the i^{th} snippet.

Following [12], we adopt the MIL-based loss as the basic objective function. Specifically, we determine the video-level prediction p_i by taking the mean value of the top- k anomaly scores. For positive bags, we set $k = \lfloor T/16 + 1 \rfloor$, and for negative bags, we set $k = 1$. Given a mini batch containing B samples with video-level ground-truth y_i , the binary cross-entropy is formulated as:

$$\mathcal{L}_{ce} = \sum_{n=1}^B -y_i \log(p_i). \quad (12)$$

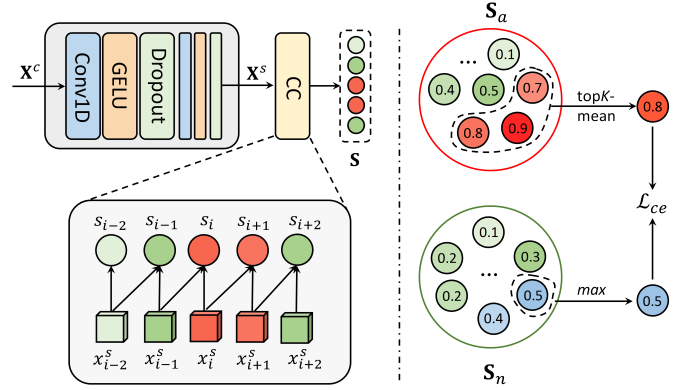


Fig. 5. Structure of MLP, CC module (left), and MIL-based loss (right).

D. Prompt-Enhanced Learning

The PEL module aims to enrich the visual representations by incorporating knowledge-based contextual information, thereby enhancing the model's ability to identify anomalies in intricate scenarios. Specifically, the PEL module comprises three steps, namely prompt construction, fore-background separation, and cross-modal alignment, depicted in Figure 6.

1) *Prompt Construction*: Considering the versatility of prompts, we first select 12 common relations from ConceptNet as the pre-retrieval semantics, followed by choosing the top five items with the highest occurrence frequency across all categories as the retrieval relations, denoted as $\{r_j\}_{j=1}^R$. The concept dictionary \mathcal{D} is then constructed by retrieving all edges of the relation r_j established with a given class c as the head or tail node. The non-category node in each edge is used as the key, and the relevance score of the edge is taken as the value. To remove noisy entries that may interfere with the semantics of anomalies, we first eliminate concepts with relevance scores less than or equal to 0 (Step 1). Next, the remaining entries are filtered by using the average of the relevance scores as the threshold (Step 2). In general, the higher the relevance score, the stronger the semantic relationship between the nodes.

After obtaining the concept dictionary, we use a pre-trained CLIP model [23] to extract the corresponding prompt representations. For a given class c , a set of keys $\{k_i^c\}_{i=1}^N$ from the concept dictionary is first extracted as the context prompt, which is then separately fed into the text encoder to extract 512-dimensional feature vectors $\{\mathbf{K}_i^c\}_{i=1}^N$. Finally, the average of all feature vectors is regarded as the knowledge-based prompt feature, denoted as follows:

$$\mathbf{T}^c = \frac{1}{N} \sum_{i=1}^N \mathbf{K}_i^c, \quad (13)$$

where N denotes the number of keys. The prompt representation incorporates relevant concepts from multiple relations and facilitates the semantic enhancement of visual features.

2) *Fore-Background Separation*: Since snippet-level features lack full contextual information, direct alignment with prompt features may result in boundary deviations of anomaly localization. Therefore, it is crucial to distinguish between class-specific foreground and class-agnostic background from

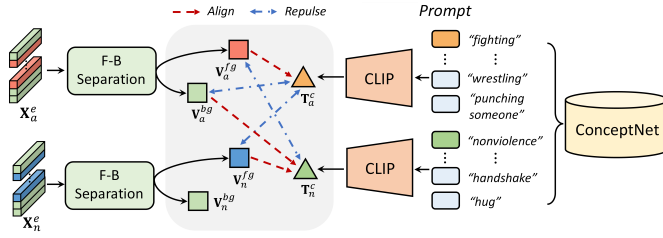


Fig. 6. Illustration of PEL module. knowledge-based prompts are first constructed via ConceptNet. Video-level foreground and background are then separated. Cross-modal alignment encourages video-prompt pairs with the same semantics to converge and form discriminative decision boundaries.

consecutive snippets. To achieve this, we utilize the scaled anomaly scores as activations to produce video-level foreground and background features, respectively, represented as follows:

$$\mathbf{A}^{fg} = \frac{\exp(\mu \mathbf{S}) - 1}{\sum_t (\exp(\mu \mathbf{S}_t) - 1)}, \quad \mathbf{V}^{fg} = \mathbf{A}^{fg} \mathbf{X}^e, \quad (14)$$

$$\mathbf{A}^{bg} = \frac{\exp(\mu \bar{\mathbf{S}}) - 1}{\sum_t (\exp(\mu \bar{\mathbf{S}}_t) - 1)}, \quad \mathbf{V}^{bg} = \mathbf{A}^{bg} \mathbf{X}^e, \quad (15)$$

where \mathbf{S}_t represents the anomaly score at the snippet-level, and μ is a predefined scaling factor that cooperates with the $\exp(\cdot)$ operation to enhance high-confidence activations. In contrast, $\bar{\mathbf{S}} = 1 - \mathbf{S}_t$ represents the normal confidence of the current snippet, and \mathbf{X}^e denotes the middle-layer output of the MLP, which shares the same dimension as \mathbf{T}^c .

3) *Cross-modal Alignment*: Finally, we present our approach to enhancing the fine-grained semantics of visual features by aligning them with the prompt features, as illustrated in Figure 7. For the abnormal video, the visual foreground \mathbf{V}_a^{fg} is aligned to its knowledge-based prompt feature \mathbf{T}_a^c , while the background \mathbf{V}_a^{bg} is aligned to the unified normal prompt \mathbf{T}_n^c . For normal video, only the alignment between the normal foreground \mathbf{V}_n^{fg} and the corresponding prompt \mathbf{T}_n^c is considered. The process is formulated as follows:

$$\psi(\mathbf{V}, \mathbf{T}) = \frac{\mathbf{V} \cdot \mathbf{T}^\top}{\|\mathbf{V}\| \|\mathbf{T}\|}, \quad (16)$$

$$p_i^{v2t}(\mathbf{V}) = \frac{\exp(\psi(\mathbf{V}, \mathbf{T})/\tau)}{\sum_{k=1}^{C+1} \exp(\psi(\mathbf{V}, \mathbf{T}_k)/\tau)}, \quad (17)$$

where $\mathbf{V} \in \{\mathbf{V}_a^{fg} \cup \mathbf{V}_a^{bg} \cup \mathbf{V}_n^{fg}\}$ and $\mathbf{T} \in \{\mathbf{T}_a^c \cup \mathbf{T}_n^c\}$ denote visual and textual representation, respectively, $C+1$ denotes C abnormal classes and 1 normal class, and τ is a temperature coefficient. The cross-modal alignment loss is computed using the Kullback-Leibler divergence, as follows:

$$\mathcal{L}_{kd} = \mathbb{E}_{p \sim p(v)} [\log p^{v2t}(v) - \log q^{v2t}(v)], \quad (18)$$

where $p^{v2t}(v)$ and $q^{v2t}(v)$ denote the similarity score and semantic consistency label of the video-prompt pair, respectively. If it is a positive pair, $q = 1$; otherwise, $q = 0$.

E. Objective Function and Score Smoothing

In the training phase, the overall objective function of our model is denoted as:

$$\mathcal{L} = \mathcal{L}_{ce} + \lambda \mathcal{L}_{kd}, \quad (19)$$

where the coefficient λ is utilized to adjust the alignment loss. By optimizing this objective function, our model acquires the ability to generate discriminative representations of positive and negative snippets, while also effectively capturing the fine-grained semantics of anomalies. As a result, the generalizability of our model in complex situations is improved.

During the testing phase, we introduce the SS module to reduce false alarms caused by frame jitter or switching. This module employs distinct pooling strategies to achieve optimal results. Given an anomaly score sequence $\{s_i\}_{i=1}^T$ and a pooling window of size κ , the smoothing process can be expressed as follows:

$$\tilde{s}_i = \frac{1}{\kappa} \sum_{i=\kappa_s}^{\kappa_e} s_i, \quad (20)$$

where κ_s and κ_e denote the start and end positions of pooling, respectively. For a moving window, we set $\kappa_s = \lfloor i/\kappa \rfloor \kappa$ and $\kappa_e = (\lfloor i/\kappa \rfloor + 1) \kappa - 1$. For a sliding window, we define $\kappa_s = i$ and $\kappa_e = i + \kappa - 1$. In cases where the score sequence is shorter than the window size, the remainder is padded with zeroes. By smoothing the prediction scores, individual biases can be effectively suppressed while further reducing the occurrence of false alarms.

IV. EXPERIMENTS

In this section, we first introduce the datasets and implementation details of our framework. Subsequently, we make a comparison between our approach and state-of-the-art methods. Finally, we assess the contribution of each component via extensive ablation studies and qualitative analysis.

A. Datasets and Evaluation Metric

We perform experiments on three challenging anomaly benchmarks, i.e., UCF-Crime [11], XD-Violence [18], and ShanghaiTech [51] datasets. Details are given as follows:

1) *UCF-Crime*: It comprises 1900 surveillance videos with a total duration of 128 hours, covering 13 real-world anomalies, including abuse, robbery, explosion, and road accidents. For the weakly supervised setting, the dataset is divided into 1610 training and 290 test videos, with only video-level annotations available for training and frame-level annotations provided for testing.

2) *XD-Violence*: It is the latest and largest multimodal violence dataset containing 4754 untrimmed videos with a total duration of 217 hours. The dataset includes 3954 training and 800 test videos from various sources such as surveillance, movies, car cameras, and games. The dataset covers six types of violence, including abuse, car accidents, explosions, fighting, riots, and shooting. Most of the videos in this dataset contain artistic expressions such as camera movements and scene switching, which poses a challenge for video anomaly detection.

3) *ShanghaiTech*: It comprises 437 videos from 13 campus scenes. The original version was used for semi-supervised anomaly detection, where the training set consisted of only normal videos. Zhong *et al.* [20] reorganized the dataset for weakly supervised setting, with 238 videos in the training set and 199 videos in the test set.

4) *Evaluation Metric*: For the UCF-Crime and ShanghaiTech datasets, we use the area under the frame-level receiver operating characteristic curve (AUC) as the evaluation metric. For the XD-Violence dataset, the area under the precision-recall curve, also known as the average precision (AP), is utilized as the standard evaluation metric. In addition, to guarantee the reliability of anomaly prediction, a false positive rate with a threshold value of 0.5, or false alarm rate (FAR), is employed for evaluation. In general, the lower the FAR, the more robust the model is to normal samples.

B. Implementation Details

1) *Data Pre-processing*: Following existing work [12], we utilize the I3D network [49] pre-trained on Kinetics-400 for feature extraction. For a fair comparison, we utilize a 10-crop augmentation strategy, consisting of the center, four corners, and their mirrored counterparts, for the UCF-Crime and ShanghaiTech datasets. In contrast, a 5-crop augmentation strategy, consisting of the center and four corners, is employed for the XD-Violence dataset as in [18].

2) *Hyperparameter settings*: The hidden dimension of the TCA module is set to 128, and the fusion weight α is initialized to 0.5. The two Conv1D layers of MLP have 512 and 300 nodes, respectively, both with a dropout rate of 0.1. For the UCF-Crime, XD-Violence, and ShanghaiTech datasets, we adopt local window sizes of 9, 9, and 5, respectively. The causal convolution kernel size Δt is set to 9, 3 and 3, respectively, while the temperature coefficient τ is initialized to 0.09, 0.05, and 0.2, respectively. The scaling factor μ for fore-background separation is set to 10, and the loss coefficient λ is set to 1 for the UCF-Crime and XD-Violence datasets, while it is set to 9 for the ShanghaiTech dataset.

3) *Training and Test Details*: During the training phase, our model is trained using the Adam optimizer [52] with a batch size of 128 and 50 epochs in total. The initial learning rate for the three datasets is set to 5×10^{-4} , with a cosine decay strategy. For the balance of computational efficiency and detection performance, the snippet sampling threshold in the training phase is set to 200 as in [18] [12] [45] [53]. In the testing phase, we apply sliding pooling with window sizes of 7 and 3 to the UCF-Crime and ShanghaiTech datasets, respectively. Moving pooling with a window size of 9 is adopted for the XD-Violence dataset. More details can be found in supplementary materials.

C. Comparison With State-of-the-Art Methods

We report the state-of-the-art results on the three benchmarks in Tables I-III. Notably, the weakly supervised-based methods exhibit superior performance compared to the semi-supervised learning methods across all datasets. The former, which solely relies on normal videos during the training phase,

TABLE I
PERFORMANCE COMPARISON OF STATE-OF-THE-ART METHODS ON THE UCF-CRIME DATASET

Supervision	Method	Feature	AUC (%)	FAR (%)
Semi-supervised	Conv-AE [5]	-	50.60	27.2
	Lu <i>et al.</i> [30]	-	65.51	3.1
	GODS [35]	BoW+TCN	70.46	2.1
Weakly-supervised	MIL-Rank [11]	C3D RGB	75.41	1.9
	IBL [54]	C3D RGB	78.66	-
	Motion-Aware [55]	PWC Flow	79.00	-
	GCN [20]	TSN RGB	82.12	0.1
	MIST [44]	I3D RGB	82.30	<u>0.13</u>
	HL-Net [18]	I3D RGB	82.44	-
	MS-BSAD [45]	I3D RGB	83.53	-
	RTFM [13]	I3D RGB	84.30	-
	CRFD [12]	I3D RGB	84.89	0.72
	DDL [53]	I3D RGB	85.12	-
	MSL [43]	I3D RGB	85.30	-
	MLAD [56]	I3D RGB	85.47	7.47
	NL-MIL [19]	I3D RGB	85.63	-
	S3R [14]	I3D RGB	85.99	-
	Zhang <i>et al.</i> [15]	I3D RGB	86.22	-
	UML [57]	X-CLIP RGB	86.75	-
UR-DMU [21]	I3D RGB	86.97	1.05	
Ours	I3D RGB	<u>86.76</u>	0.43	

TABLE II
PERFORMANCE COMPARISON OF STATE-OF-THE-ART METHODS ON THE XD-VIOLENCE DATASET

Supervision	Method	Feature	AP (%)	FAR (%)
Semi-supervised	SVM baseline	-	50.78	-
	OCSVM [58]	-	27.25	-
	Conv-AE [5]	-	30.77	-
Weakly-supervised	MIL-Rank [11]	C3D RGB	73.20	-
	HL-Net [18]	I3D RGB	75.44	-
	CA-VAD [59]	I3D RGB	76.90	-
	RTFM [13]	I3D RGB	77.81	-
	CRFD [12]	I3D RGB	75.90	-
	DDL [53]	I3D RGB	80.72	-
	MSL [43]	I3D RGB	78.28	-
	NL-MIL [19]	I3D RGB	78.51	-
	S3R [14]	I3D RGB	80.26	-
	UR-DMU [21]	I3D RGB	<u>81.66</u>	<u>0.65</u>
	Zhang <i>et al.</i> [15]	I3D+VGGish	81.43	-
CMA-LA [60]	I3D+VGGish	83.54	-	
MACIL-SD [61]	I3D+VGGish	83.40	-	
Ours	I3D RGB	85.59	0.57	

is susceptible to higher false alarms. This is primarily due to the weak generalization of these methods to unseen samples. On the other hand, the latter enables the model to learn discriminative patterns of both normal and abnormal samples, thus leading to better detection performance.

Our model achieves competitive results across three datasets among all weakly supervised methods. Although our model's AUC value on the UCF-Crime dataset is lower than that of UR-DMU [21] by 0.21%, we outperform UR-DMU on the XD-Violence dataset with an absolute gain of 3.93% AP and lower false alarm rates on both datasets. UR-DMU employs an additional encoder layer to learn local features with temporal masks, whereas our TCA module achieves local-global context modeling by reusing the similarity matrix. Additionally, UR-DMU introduces a dual memory unit to

TABLE III
PERFORMANCE COMPARISON OF STATE-OF-THE-ART METHODS ON THE SHANGHAITECH DATASET

Supervision	Method	Feature	AUC (%)	FAR (%)
Semi-supervised	Mem-AE [6]	-	71.20	-
	HF ² -VAD [62]	-	76.20	-
	DLAN-AC [63]	-	74.70	-
Weakly-supervised	MIL-Rank [11]	C3D RGB	86.30	0.15
	IBL [54]	C3D RGB	82.50	0.10
	GCN [20]	TSN RGB	84.44	-
	CLAWS [64]	C3D RGB	89.67	-
	AR-Net [42]	RGB+Flow	91.24	0.10
	MIST [44]	I3D RGB	94.83	<u>0.05</u>
	CRFD [12]	I3D RGB	<u>97.48</u>	-
	RTFM [13]	I3D RGB	97.21	-
	MSL [43]	VideoSwin	97.32	-
	NL-MIL [19]	I3D RGB	97.43	-
	S3R [14]	I3D RGB	<u>97.48</u>	-
	UML [57]	X-CLIP RGB	96.78	-
	Ours	I3D RGB	98.14	0.00

TABLE IV
THE CONTRIBUTION OF EACH COMPONENT. TCA: TEMPORAL CONTEXT AGGREGATION. PEL: PROMPT-ENHANCED LEARNING. SS: SCORE SMOOTHING.

Baseline	TCA	PEL	SS	UCF	XD	SHTech
				AUC (%)	AP (%)	AUC (%)
✓	✗	✗	✗	82.50	73.51	92.25
✓	✓	✗	✗	85.72	83.28	97.82
✓	✓	✓	✗	86.36	85.26	98.00
✓	✓	✓	✓	86.76	85.59	98.14

store normal and abnormal patterns and enlarges the decision boundary through a magnitude distance loss. In contrast, our proposed PEL module enhances fine-grained detection performance by considering the intra-class discriminability of exceptions while ensuring inter-class separability. Notably, our model even outperforms multimodal-based approaches, namely CMA-LA [60] and MACIL-SD [61], with 2.19% and 2.05% gains on the XD-violence dataset, respectively. Although the PEL module requires extra textual information in the training phase, our model only requires appearance features as input during inference. Furthermore, our model achieves a new state-of-the-art performance on the ShanghaiTech dataset, with a 0.66% improvement in AUC compared to the S3R [14] and CRFD [12] methods. For the first time, the false alarm rate is also reduced to 0, indicating that the model has sufficient confidence and robustness for normal samples.

D. Ablation Studies

In this subsection, we perform extensive ablation studies to verify the contribution of each component of our model.

1) *Contribution of Each Component*: Table IV presents the contributions of each component, where ‘Baseline’ refers to the combination of MLP and CC module. Significantly, the TCA module is responsible for the primary improvement, delivering AUC gains of 9.77% and 5.57% on the ShanghaiTech and XD-Violence datasets, respectively, highlighting the need for context modeling. Furthermore, the introduction of the PEL module enhances the detection performance of

TABLE V
CONTRIBUTION OF INTERNAL COMPONENTS OF THE TCA MODULE. DPE: DYNAMIC POSITION ENCODING.

Baseline	Local	Global	DPE	UCF	XD	SHTech
				AUC (%)	AP (%)	AUC (%)
✓	✗	✗	✗	82.50	73.51	92.25
✓	✓	✗	✗	84.64	77.29	92.79
✓	✗	✓	✗	82.30	80.80	85.65
✓	✓	✓	✗	85.18	83.05	97.62
✓	✓	✓	✓	85.72	83.28	97.82

TABLE VI
THE SUPERIORITY OF ADAPTIVE FUSION IN THE TCA MODULE.

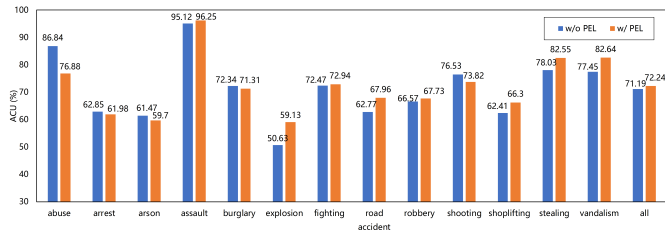
Weight	Global	Local	UCF	XD	SHTech
			AUC (%)	AP (%)	AUC (%)
Fixed	0.1	0.9	84.82	77.57	97.74
	0.3	0.7	85.07	81.08	97.57
	0.5	0.5	85.17	82.45	97.71
	0.7	0.3	85.24	82.53	97.56
	0.9	0.1	84.85	80.57	97.60
Learnable	α	$1 - \alpha$	85.72	83.28	97.82

TABLE VII
COMPARISON OF DIFFERENT NORMALIZATION METHODS FOR ADAPTIVE FUSION

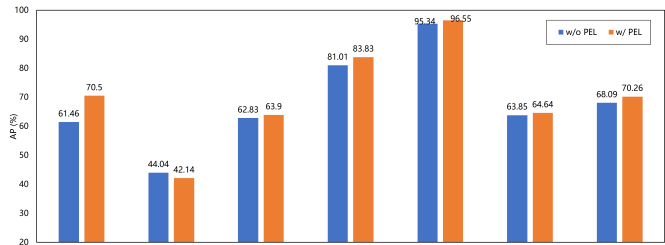
Normalization	UCF	XD	SHTech
	AUC (%)	AP (%)	AUC (%)
None	83.44	83.28	94.06
Power Norm	82.88	79.04	94.52
L2 Norm	85.09	73.92	97.48
Power + L2 Norm	85.72	71.13	97.82

our model on all three datasets, with a substantial AP gain of 1.98% on XD-Violence. We contend that this is due to the internal distribution characteristics of the dataset, which has a wider range of acquisition sources than surveillance videos such as UCF-Crime and ShanghaiTech, resulting in diverse and complex video content. Finally, the SS module further improves the detection performance of our model by 0.4%, 0.33%, and 0.14% on the three benchmarks, respectively, demonstrating the effectiveness and generality of the module.

2) *Contribution of Components of the TCA module*: Table V demonstrates that local context modeling can effectively improve the detection performance of our baseline. However, global context modeling resulted in a significant degradation of performance on the UCF-Crime and ShanghaiTech datasets, while outperforming local context modeling on XD-Violence. We assert that global context modeling introduces long-range noise to fixed surveillance videos, leading to reduced discrimination among snippet features. In contrast, film and TV videos require a global receptive field to capture complex semantics across snippets. The adaptive fusion of local and global contexts significantly enhanced the model’s performance, indicating that each approach plays a complementary role to the other, which outperformed the baseline by 9.54% and 5.37% on the XD-Violence and ShanghaiTech datasets, respectively. Finally, the improvement from DPE indicates the importance of relative distance as a location prior.



(a) AUC results w.r.t. sub-classes on UCF-Crime.



(b) AP results w.r.t. sub-classes on XD-Violence.

Fig. 7. Contribution of the PEL module to fine-grained anomaly detection.

TABLE VIII
CONTRIBUTION OF NODE FILTERING IN PROMPT CONSTRUCTION

Method	UCF-Crime AUC (%)	XD-Violence AP (%)
None	85.34	84.35
step 1	85.87	84.61
step 1 + step 2 (fixed threshold)	86.31	85.10
step 1 + step 2 (dynamic threshold)	86.36	85.26

Next, we report the superiority of adaptive fusion in Table VI. Compared with fixed weights, the learned weights yield better results across all three datasets, which enables the dynamic adjustment of the fusion ratio of the local-global context to suit diverse datasets. Table VII compares the performance of different normalization methods. The combination of power normalization and L2 normalization achieves the best results on UCF-Crime and ShanghaiTech. However, we observe that either power normalization or L2 normalization leads to a significant drop in performance for XD-Violence. We argue that normalization may jeopardize the diversity distribution of this dataset since it contains videos from different sources and types. While normalization is necessary for surveillance videos with fixed lenses, we remove the normalization operation in adaptive fusion for XD-Violence.

3) *Contribution of Components of the PEL*: First, we investigate the effectiveness of threshold filtering in prompt construction, as presented in Table VIII. Specifically, ‘step 1’ denotes the removal of entries with relevance scores not greater than 0, while ‘step 2’ filters the remaining entries by a specific threshold. The results reveal that ‘step 1’ improves the detection performance by 0.53% and 0.26% on the UCF-Crime and XD-Violence datasets, respectively, compared with that before filtering. Moreover, ‘step 2’ with dynamic threshold further enhances the performance on both datasets, indicating the successful removal of redundant entries. The dynamic threshold

TABLE IX
PERFORMANCE COMPARISON OF DIFFERENT PROMPT TEMPLATE

Prompt Template	UCF-Crime AUC (%)	XD-Violence AP (%)
{label}	85.95	84.69
{‘a video of’ + label}	85.55	84.51
{‘a long video of’ + label}	85.63	84.59
{label + WordNet Definition} [47]	85.92	84.14
{Learnable Prompt + label} [26]	85.48	84.48
{label + ConceptNet Relation}	86.36	85.26

TABLE X
CONTRIBUTION OF FORE-BACKGROUND SEPARATION IN THE PEL MODULE

Method	UCF-Crime AUC (%)	XD-Violence AP (%)
w/o F-B separation	85.71	79.79
w/ F-B separation	86.36	85.26

TABLE XI
CONTRIBUTION OF SCORE SMOOTHING MODULE

Method	UCF AUC (%)	XD AP (%)	SHTech AUC (%)
None	86.36	85.26	98
moving window	86.65	85.59	98.03
sliding window	86.76	85.56	98.14

ensures the completeness of relevant semantic relationships to a certain extent while the fixed threshold may introduce low-relevance nodes with potentially anomalous semantics.

We also compare different prompt templates in Table IX. Using category labels as prompt templates improves the detection performance by 0.23% and 1.41% on the UCF-Crime and XD-Violence datasets, respectively, outperforming the hand-crafted templates (the 2nd and 3rd rows) and WordNet definitions (the 4th row). However, our ConceptNet-based prompts outperform the label-only prompts by 0.41% and 0.57% on the two benchmarks, respectively. Retrieving class-specific concepts based on semantic relations facilitates the mining of potential co-occurring anomalous items, while threshold filtering ensures strongly related semantic concepts, aiding the capture of fine-grained visual information.

Finally, we investigate the contribution of foreground-background separation, as presented in Table X. ‘w/o F-B separation’ denotes the mean pooling operation of snippet features and alignment with the corresponding prompt features, which leads to a significant performance degradation. The mean pooling operation weakens the anomalous region and introduces extra background noise, resulting in a biased cross-modal alignment. Foreground-background separation effectively suppresses background interference, ensuring semantic consistency between visual foreground and prompt representations.

4) *Contribution of PEL to Fine-grained Anomaly Detection*: We report the detection results of different anomaly subclasses after cross-modal alignment in Figure 7. For the UCF-Crime dataset, over half of the categories demonstrated improvements

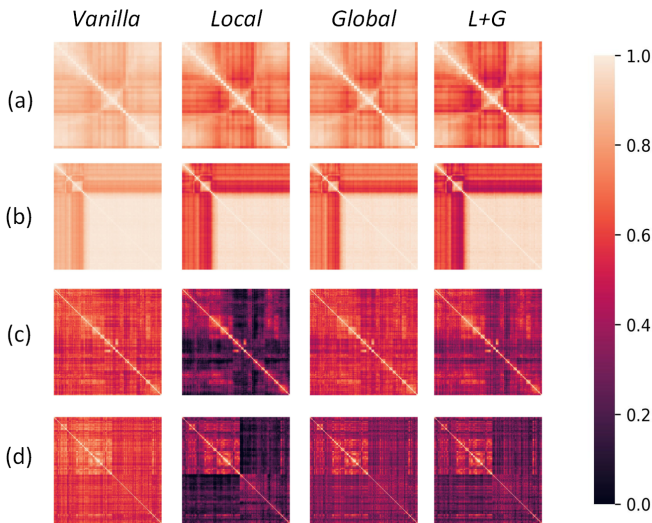


Fig. 8. Visualization of cosine similarity of context features. (a) and (b) are videos from the UCF-Crime dataset. (c) and (d) are videos from the XD-Violence dataset.

in AUC, with ‘explosion’ gaining 8.5% and ‘vandalism’ gaining 5.19%. However, some subclasses experienced significant drops in performance, with ‘abuse’ decreasing by 9.96% and ‘shooting’ by 2.71%. We discovered that ConceptNet’s relevant entries include ‘disrespect’, ‘vituperation’, and ‘scurriosity’, while the term ‘abuse’ in UCF-Crime refers to the mistreatment of animals by humans. We contend that the polysemy of English words results in a deviation of the visual representation from the original context after cross-modal alignment. Overall, the macro-AUC of the 13 subclasses of the UCF-Crime dataset increased by 1.05%.

For the XD-Violence dataset, all subclasses except for ‘car accident’ demonstrated varying degrees of increase in AP. Interestingly, the AP of ‘abuse’ increased significantly by 9.04%, which is the opposite of the UCF-Crime dataset. This is due to the former being richer in video types, including verbal and physical conflicts between characters, which is consistent with the concept of nodes extracted by ConceptNet. Furthermore, the mAP of all 6 anomaly subclasses improved by 2.17%, further supporting the contribution of cross-modal alignment to fine-grained anomaly detection.

5) *Contribution of SS*: Table XI illustrates the impact of various pooling windows in the SS module. The utilization of both moving and sliding pooling techniques effectively enhances the model’s performance while simultaneously reducing the false alarm rate. The ShanghaiTech and UCF-Crime datasets exhibit favorable outcomes with the latter, whereas the former yields superior results for the XD-Violence dataset.

E. Analysis of Time–Space Complexity

In this subsection, we compared the performance and efficiency with recent temporal modeling methods, as shown in Table XII. To ensure a fair comparison, we reproduce existing modules using open-source code and embed them in our baseline. Specifically, HL-Net [18] models global and local relationships separately using two parallel graph convolutional

TABLE XII
COMPARISON OF THE SPATIO-TEMPORAL COMPLEXITY OF DIFFERENT METHODS

Method	# Params	# FLOPS	UCF-Crime	XD-Violence
			AUC(%)	AP(%)
HL-Net [†] [18]	0.66M	133M	83.12	79.58
MTCM [†] [45]	13.27M	2.653G	83.15	78.92
RTFM [†] [13]	24.72M	791M	84.30	77.81
LA-Net [53]	2.69M	538M	83.67	79.18
LGTE [†] [65]	1.21M	241M	84.34	79.07
TCA	1.21M	241M	85.72	83.28

[†] refers to re-implementation in our baseline.

networks and concatenates the features for fusion. MTCM [45] employs multiple 1D convolution layers to capture multi-scale context information, while RTFM [13] captures multi-level temporal relations using a self-attention mechanism with a pyramid dilated convolution block. However, these multi-branch structures unavoidably introduce additional parameters and computation costs. Despite maintaining the same space-time complexity as the LGTE [65], our TCA module outperforms the former by 1.38% and 4.21% on the UCF-Crime and XD-Violence datasets, respectively. We argue that although LGTE uses channel grouping to improve encoding efficiency, it may compromise the complete semantics of feature channels. In contrast, the TCA module preserves contextual continuity by reusing the similarity matrix, and adaptive aggregation and dynamic positional coding further enhance the discriminative nature of snippet features. Notably, the feature extraction model I3D can achieve a processing speed of 263 FPS on a single Tesla A40 GPU when the input frame resolution is set to 224×224 . Subsequently, the anomaly detection model outputs anomaly scores at 350 FPS (2.9 ms), striking a good balance between detection performance and inference efficiency.

F. Qualitative Results

We first visualize the correlation of context features to demonstrate the encoding performance of the TCA module. As shown in Figure 8, the heatmap demonstrates the cosine similarity between the snippets, where the first two rows are test videos of UCF-Crime and the last two rows are from XD-Violence. We observe that 1) the variability of UCF-Crime videos is less pronounced than that of XD-Violence since the former is captured from fixed surveillance while the latter contains complex scene and camera changes; 2) local features are more discriminable than global features because the latter introduces more long-range noise; and 3) local-global aggregated features can effectively suppress redundancies and further enhance the discriminability among snippets.

To further illustrate the efficacy of the PEL module, we utilize t-SNE to visualize the features of the middle layer of the MLP. As depicted in Figure 9, the distribution of test samples in the UCF-Crime dataset appears disorderly prior to alignment, whereas the samples in the XD-Violence dataset exhibit a discernible clustering pattern. We contend that the

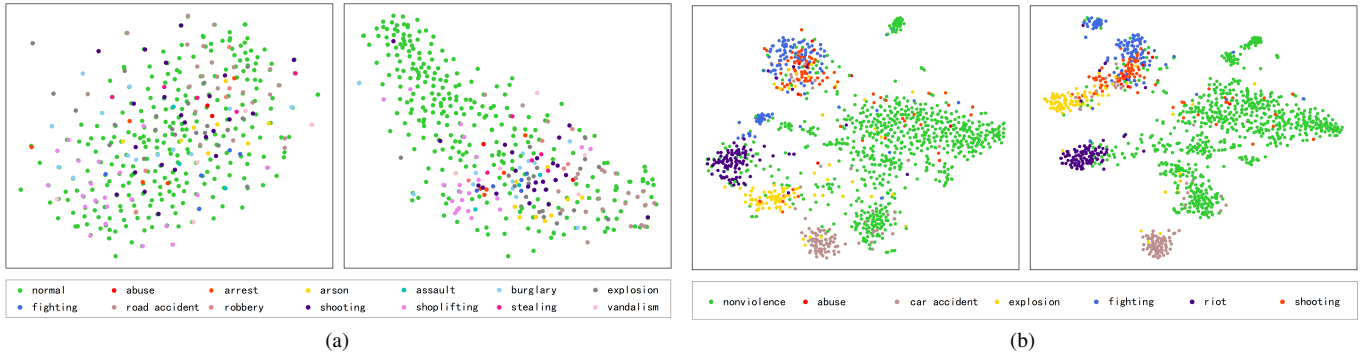


Fig. 9. Distribution of discriminative features before and after PEL using t-SNE. (a) the UCF-Crime dataset. (b) the XD-Violence dataset.

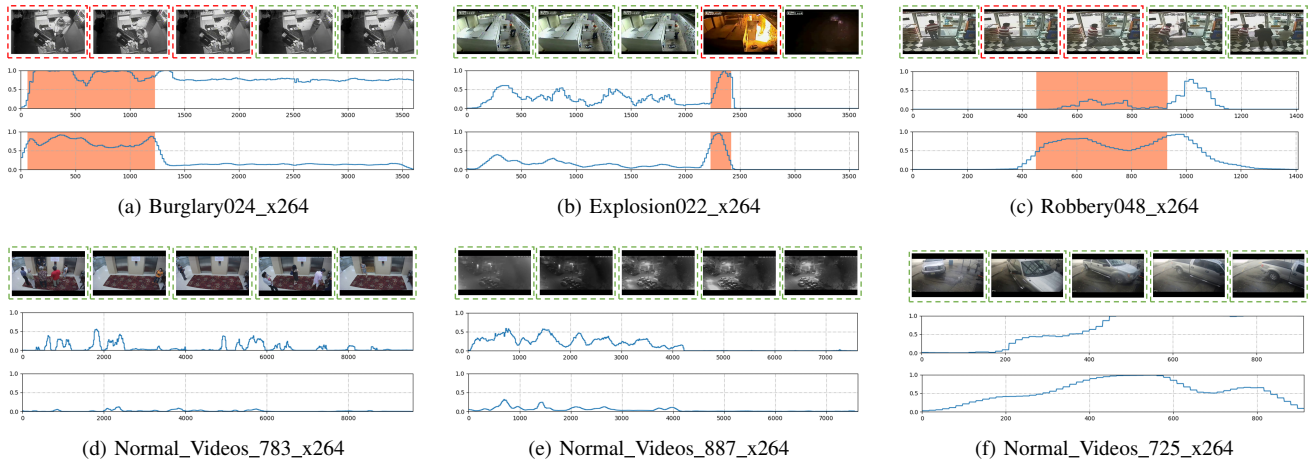


Fig. 10. Qualitative results of our method on the UCF-Crime dataset. The green and red boxes represent normal and abnormal keyframes, respectively. The second and third rows indicate the results of ‘w/ TCA’ and ‘w/ PEL & SS’, respectively. (a)-(e) are correct videos and (f) is a false alarm sample.

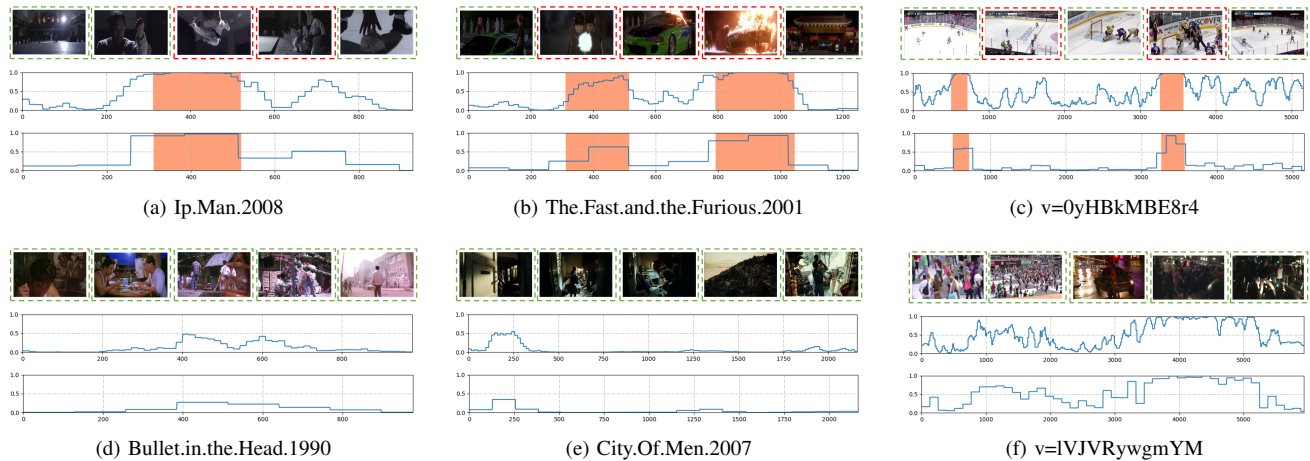


Fig. 11. Qualitative results of our method on the XD-Violence dataset. The green and red boxes represent normal and abnormal keyframes, respectively. The second and third rows indicate the results of ‘w/ TCA’ and ‘w/ PEL & SS’, respectively. (a)-(e) are correct videos and (f) is a false alarm sample.

former surveillance videos possess temporal coherence, resulting in blurred fore-background boundaries. Conversely, the latter videos have natural shot boundaries created by artificial means, leading to a more distinguishable boundary. Through the incorporation of cross-modal alignment loss, abnormal foregrounds converge towards the corresponding prompt fea-

tures to form compact clusters. In contrast, hard-negative snippets and backgrounds align with a uniform normal center, consequently increasing the relative distance between abnormal and normal snippets in the embedding space. Noteworthy is that distinct fine-grained anomalous samples are effectively differentiated, surpassing current binary classification models

in terms of semantic representation.

Finally, we report the anomaly scores of several test videos in Figures 10 and 11. The second row displays the detection results of the TCA module, while the third row shows the outcomes of PEL and SS. Compared to TCA, the introduction of PEL and SS can achieve more accurate anomaly localization results, which can be attributed to the effective suppression of non-anomaly noise through F-B separation in PEL. Meanwhile, false alarms triggered by in/out-of-frames and luminance changes are corrected, thereby further reducing the false alarm rate in normal videos. Our model can be adapted to multiple scenarios and types of anomalous event detection, owing to the rich semantic information provided by the prompt for context features.

V. CONCLUSION

In this paper, we focus on efficient temporal context modeling and semantic enhancement of visual features for weakly supervised video anomaly detection. Our model achieves local-global context aggregation through the reuse of the similarity matrix and introduces knowledge-based prompts to enhance the weak semantic discriminability of context features. The incorporation of context information and external knowledge significantly improves the accuracy of anomaly localization. In addition, we implemented score smoothing to reduce individual bias in continuous sequences and reduce false alarms. The results of extensive experiments demonstrate that our model performs competitively on three benchmarks with fewer parameters and computational cost. Additionally, the detection accuracy of several abnormal sub-classes is significantly improved. In the future, multimodal information such as motion and audio remains to be explored, and open-set anomaly detection also deserves attention.

ACKNOWLEDGMENTS

This work was supported by the state key development program in the 14th Five-Year under Grant No.2021YFF0900701, 2021YFF0602103, 2021YFF0602102, 2021QY1702, and in part by National Natural Science Foundation of China (No.61801441). We also thank the research funds under Grant No.2019QG0001 from the Institute for Guo Qiang, Tsinghua University, and the High-quality and Cutting-edge Disciplines Construction Project for Universities in Beijing (Internet Information, Communication University of China).

REFERENCES

- [1] A. Adam, E. Rivlin, I. Shimshoni, and D. Reinitz, "Robust real-time unusual event detection using multiple fixed-location monitors," *IEEE Trans. Pattern Anal. Mach. Intell.*, vol. 30, no. 3, pp. 555–560, Mar. 2008.
- [2] V. Chandola, A. Banerjee, and V. Kumar, "Anomaly detection: A survey," *ACM Comput. Surv.*, vol. 41, no. 3, pp. 1–58, Jul. 2009.
- [3] Y. Benezeth, P.-M. Jodoin, V. Saligrama, and C. Rosenberger, "Abnormal events detection based on spatio-temporal co-occurrences," in *IEEE Conf. Comput. Vis. Pattern Recognit. (CVPR)*, Jun. 2009, pp. 2458–2465.
- [4] G. Pang, C. Shen, L. Cao, and A. V. D. Hengel, "Deep learning for anomaly detection: A review," *ACM Comput. Surv.*, vol. 54, no. 2, pp. 1–38, Mar. 2021.
- [5] M. Hasan, J. Choi, J. Neumann, A. K. Roy-Chowdhury, and L. S. Davis, "Learning temporal regularity in video sequences," in *IEEE Conf. Comput. Vis. Pattern Recognit. (CVPR)*, Jun. 2016, pp. 733–742.
- [6] D. Gong, L. Liu, V. Le, B. Saha, M. R. Mansour, S. Venkatesh, and A. V. D. Hengel, "Memorizing normality to detect anomaly: Memory-augmented deep autoencoder for unsupervised anomaly detection," in *Proc. IEEE/CVF Int. Conf. Comput. Vis. (ICCV)*, Oct. 2019, pp. 1705–1714.
- [7] H. Park, J. Noh, and B. Ham, "Learning memory-guided normality for anomaly detection," in *IEEE/CVF Conf. Comput. Vis. Pattern Recognit. (CVPR)*, Jun. 2020, pp. 14 360–14 369.
- [8] W. Luo, W. Liu, D. Lian, J. Tang, L. Duan, X. Peng, and S. Gao, "Video anomaly detection with sparse coding inspired deep neural networks," *IEEE Trans. Pattern Anal. Mach. Intell.*, vol. 43, no. 3, pp. 1070–1084, Mar. 2021.
- [9] C. Chen, Y. Xie, S. Lin, A. Yao, G. Jiang, W. Zhang, Y. Qu, R. Qiao, B. Ren, and L. Ma, "Comprehensive regularization in a bi-directional predictive network for video anomaly detection," in *Proc. AAAI Conf. Artif. Intell.*, vol. 36, no. 1, Jun. 2022, pp. 230–238.
- [10] L. Wang, J. Tian, S. Zhou, H. Shi, and G. Hua, "Memory-augmented appearance-motion network for video anomaly detection," *Pattern Recognit.*, vol. 138, p. 109335, Jun. 2023.
- [11] W. Sultani, C. Chen, and M. Shah, "Real-world anomaly detection in surveillance videos," in *IEEE/CVF Conf. Comput. Vis. Pattern Recognit. (CVPR)*, Jun. 2018, pp. 6479–6488.
- [12] P. Wu and J. Liu, "Learning causal temporal relation and feature discrimination for anomaly detection," *IEEE Trans. Image Process.*, vol. 30, pp. 3513–3527, 2021.
- [13] Y. Tian, G. Pang, Y. Chen, R. Singh, J. W. Verjans, and G. Carneiro, "Weakly-supervised video anomaly detection with robust temporal feature magnitude learning," in *Proc. IEEE/CVF Int. Conf. Comput. Vis. (ICCV)*, Oct. 2021, pp. 4955–4966.
- [14] J.-C. Wu, H.-Y. Hsieh, D.-J. Chen, C.-S. Fuh, and T.-L. Liu, "Self-supervised sparse representation for video anomaly detection," in *Proc. Eur. Conf. Comput. Vis. (ECCV)*, 2022, pp. 729–745.
- [15] C. Zhang, G. Li, Y. Qi, S. Wang, L. Qing, Q. Huang, and M.-H. Yang, "Exploiting completeness and uncertainty of pseudo labels for weakly supervised video anomaly detection," *arXiv preprint arXiv:2212.04090*, 2022.
- [16] M. Defferrard, X. Bresson, and P. Vandergheynst, "Convolutional neural networks on graphs with fast localized spectral filtering," in *Proc. Adv. Neural Inf. Process. Syst.*, vol. 29, 2016, pp. 3837–3845.
- [17] A. Vaswani, N. Shazeer, N. Parmar, J. Uszkoreit, L. Jones, A. N. Gomez, Ł. Kaiser, and I. Polosukhin, "Attention is all you need," in *Proc. Adv. Neural Inf. Process. Syst.*, vol. 30, 2017, pp. 5998–6008.
- [18] P. Wu, J. Liu, Y. Shi, Y. Sun, F. Shao, Z. Wu, and Z. Yang, "Not only look, but also listen: Learning multimodal violence detection under weak supervision," in *Proc. Eur. Conf. Comput. Vis. (ECCV)*, 2020, pp. 322–339.
- [19] S. Park, H. Kim, M. Kim, D. Kim, and K. Sohn, "Normality guided multiple instance learning for weakly supervised video anomaly detection," in *Proc. IEEE Winter Conf. Appl. Comput. Vis. (WACV)*, Jan. 2023, pp. 2664–2673.
- [20] J.-X. Zhong, N. Li, W. Kong, S. Liu, T. H. Li, and G. Li, "Graph convolutional label noise cleaner: Train a plug-and-play action classifier for anomaly detection," in *IEEE/CVF Conf. Comput. Vis. Pattern Recognit. (CVPR)*, Jun. 2019, pp. 1237–1246.
- [21] H. Zhou, J. Yu, and W. Yang, "Dual memory units with uncertainty regulation for weakly supervised video anomaly detection," *arXiv preprint arXiv:2302.05160*, 2023.
- [22] P. Liu, W. Yuan, J. Fu, Z. Jiang, H. Hayashi, and G. Neubig, "Pre-train, prompt, and predict: A systematic survey of prompting methods in natural language processing," *ACM Comput. Surv.*, vol. 55, no. 9, pp. 1–35, Jan. 2023.
- [23] A. Radford, J. W. Kim, C. Hallacy, A. Ramesh, G. Goh, S. Agarwal, G. Sastry, A. Askell, P. Mishkin, J. Clark *et al.*, "Learning transferable visual models from natural language supervision," in *Proc. IEEE Int. Conf. Mach. Learn. (ICML)*, 2021, pp. 8748–8763.
- [24] M. Wang, J. Xing, and Y. Liu, "Actionclip: A new paradigm for video action recognition," *arXiv preprint arXiv:2109.08472*, 2021.
- [25] K. Zhou, J. Yang, C. C. Loy, and Z. Liu, "Learning to prompt for vision-language models," *Int. J. Comput. Vis.*, vol. 130, no. 9, pp. 2337–2348, Jul. 2022.
- [26] C. Ju, T. Han, K. Zheng, Y. Zhang, and W. Xie, "Prompting visual-language models for efficient video understanding," in *Proc. Eur. Conf. Comput. Vis. (ECCV)*, 2022, pp. 105–124.
- [27] R. Speer, J. Chin, and C. Havasi, "ConceptNet 5.5: An open multilingual graph of general knowledge," in *Proc. AAAI Conf. Artif. Intell.*, vol. 31, no. 1, Feb. 2017, pp. 4444–4451.

- [28] R. Mehran, A. Oyama, and M. Shah, "Abnormal crowd behavior detection using social force model," in *IEEE Conf. Comput. Vis. Pattern Recognit. (CVPR)*, Jun. 2009, pp. 935–942.
- [29] B. Zhao, L. Fei-Fei, and E. P. Xing, "Online detection of unusual events in videos via dynamic sparse coding," in *IEEE Conf. Comput. Vis. Pattern Recognit. (CVPR)*, Jun. 2011, pp. 3313–3320.
- [30] C. Lu, J. Shi, and J. Jia, "Abnormal event detection at 150 FPS in MATLAB," in *Proc. IEEE Int. Conf. Comput. Vis. (ICCV)*, Dec. 2013, pp. 2720–2727.
- [31] W. Li, V. Mahadevan, and N. Vasconcelos, "Anomaly detection and localization in crowded scenes," *IEEE Trans. Pattern Anal. Mach. Intell.*, vol. 36, no. 1, pp. 18–32, Jan. 2014.
- [32] D. Xu, Y. Yan, E. Ricci, and N. Sebe, "Detecting anomalous events in videos by learning deep representations of appearance and motion," *Comput. Vis. Image Underst.*, vol. 156, pp. 117–127, Mar. 2017.
- [33] M. Sabokrou, M. Khalooei, M. Fathy, and E. Adeli, "Adversarially learned one-class classifier for novelty detection," in *IEEE/CVF Conf. Comput. Vis. Pattern Recognit. (CVPR)*, Jun. 2018, pp. 3379–3388.
- [34] P. Wu, J. Liu, and F. Shen, "A deep one-class neural network for anomalous event detection in complex scenes," *IEEE Trans. Neural Netw. Learn. Syst.*, pp. 1–14, 2019.
- [35] J. Wang and A. Cherian, "GODS: Generalized one-class discriminative subspaces for anomaly detection," in *Proc. IEEE Int. Conf. Comput. Vis. (ICCV)*, Oct. 2019, pp. 8200–8210.
- [36] W. Liu, W. Luo, D. Lian, and S. Gao, "Future frame prediction for anomaly detection - a new baseline," in *IEEE/CVF Conf. Comput. Vis. Pattern Recognit. (CVPR)*, Jun. 2018, pp. 6536–6545.
- [37] M. Z. Zaheer, J.-H. Lee, M. Astrid, and S.-I. Lee, "Old is gold: Redefining the adversarially learned one-class classifier training paradigm," in *IEEE/CVF Conf. Comput. Vis. Pattern Recognit. (CVPR)*, Jun. 2020, pp. 14 171–14 181.
- [38] J. R. Medel and A. Savakis, "Anomaly detection in video using predictive convolutional long short-term memory networks," *arXiv preprint arXiv:1612.00390*, 2016.
- [39] O. Ronneberger, P. Fischer, and T. Brox, "U-net: Convolutional networks for biomedical image segmentation," in *Lecture Notes in Computer Science*. Springer International Publishing, 2015, pp. 234–241.
- [40] I. Goodfellow, J. Pouget-Abadie, M. Mirza, B. Xu, D. Warde-Farley, S. Ozair, A. Courville, and Y. Bengio, "Generative adversarial networks," *Commun. ACM*, vol. 63, no. 11, pp. 139–144, Oct. 2020.
- [41] X. Shi, Z. Chen, H. Wang, D.-Y. Yeung, W.-K. Wong, and W.-c. Woo, "Convolutional lstm network: A machine learning approach for precipitation nowcasting," in *Proc. Adv. Neural Inf. Process. Syst.*, vol. 28, 2015, pp. 802–810.
- [42] B. Wan, Y. Fang, X. Xia, and J. Mei, "Weakly supervised video anomaly detection via center-guided discriminative learning," in *Proc. IEEE Int. Conf. Multimedia Expo (ICME)*, Jul. 2020, pp. 1–6.
- [43] S. Li, F. Liu, and L. Jiao, "Self-training multi-sequence learning with transformer for weakly supervised video anomaly detection," in *Proc. AAAI Conf. Artif. Intell.*, vol. 36, no. 2, 2022, pp. 1395–1403.
- [44] J.-C. Feng, F.-T. Hong, and W.-S. Zheng, "MIST: Multiple instance self-training framework for video anomaly detection," in *IEEE/CVF Conf. Comput. Vis. Pattern Recognit. (CVPR)*, Jun. 2021, pp. 14 009–14 018.
- [45] Y. Zhen, Y. Guo, J. Wei, X. Bao, and D. Huang, "Multi-scale background suppression anomaly detection in surveillance videos," in *Proc. IEEE Int. Conf. Image Process. (ICIP)*, Sep. 2021, pp. 1114–1118.
- [46] T. Gao, A. Fisch, and D. Chen, "Making pre-trained language models better few-shot learners," *arXiv preprint arXiv:2012.15723*, 2020.
- [47] L. Yao, J. Han, Y. Wen, X. Liang, D. Xu, W. Zhang, Z. Li, C. Xu, and H. Xu, "Detclip: Dictionary-enriched visual-concept paralleled pre-training for open-world detection," *arXiv preprint arXiv:2209.09407*, 2022.
- [48] G. A. Miller, "WordNet," *Commun. ACM*, vol. 38, no. 11, pp. 39–41, Nov. 1995.
- [49] J. Carreira and A. Zisserman, "Quo vadis, action recognition? a new model and the kinetics dataset," in *IEEE Conf. Comput. Vis. Pattern Recognit. (CVPR)*, Jul. 2017, pp. 4724–4733.
- [50] Z. Yu, J. Yu, J. Fan, and D. Tao, "Multi-modal factorized bilinear pooling with co-attention learning for visual question answering," in *Proc. IEEE Int. Conf. Comput. Vis. (ICCV)*, Oct. 2017, pp. 1839–1848.
- [51] W. Luo, W. Liu, and S. Gao, "A revisit of sparse coding based anomaly detection in stacked RNN framework," in *Proc. IEEE Int. Conf. Comput. Vis. (ICCV)*, Oct. 2017, pp. 341–349.
- [52] D. P. Kingma and J. Ba, "Adam: A method for stochastic optimization," *arXiv preprint arXiv:1412.6980*, 2014.
- [53] Y. Pu and X. Wu, "Locality-aware attention network with discriminative dynamics learning for weakly supervised anomaly detection," in *Proc. IEEE Int. Conf. Multimedia Expo (ICME)*, Jul. 2022, pp. 1–6.
- [54] J. Zhang, L. Qing, and J. Miao, "Temporal convolutional network with complementary inner bag loss for weakly supervised anomaly detection," in *Proc. IEEE Int. Conf. Image Process. (ICIP)*, Sep. 2019, pp. 4030–4034.
- [55] Y. Zhu and S. Newsam, "Motion-aware feature for improved video anomaly detection," in *Proc. Brit. Mach. Vis. Conf. (BMVC)*, 2019, p. 270.
- [56] C. Zhang, G. Li, Q. Xu, X. Zhang, L. Su, and Q. Huang, "Weakly supervised anomaly detection in videos considering the openness of events," *IEEE Trans. Intell. Transp. Syst.*, vol. 23, no. 11, pp. 21 687–21 699, Nov. 2022.
- [57] H. Lv, Z. Yue, Q. Sun, B. Luo, Z. Cui, and H. Zhang, "Unbiased multiple instance learning for weakly supervised video anomaly detection," *arXiv preprint arXiv:2303.12369*, 2023.
- [58] B. Schölkopf, R. C. Williamson, A. Smola, J. Shawe-Taylor, and J. Platt, "Support vector method for novelty detection," in *Proc. Adv. Neural Inf. Process. Syst.*, vol. 12, 1999, pp. 582–588.
- [59] S. Chang, Y. Li, S. Shen, J. Feng, and Z. Zhou, "Contrastive attention for video anomaly detection," *IEEE Trans. Multimedia*, vol. 24, pp. 4067–4076, 2022.
- [60] Y. Pu and X. Wu, "Audio-guided attention network for weakly supervised violence detection," in *Proc. IEEE Int. Conf. Consum. Electron. Comput. Eng. (ICCECE)*, Jan. 2022, pp. 219–223.
- [61] J. Yu, J. Liu, Y. Cheng, R. Feng, and Y. Zhang, "Modality-aware contrastive instance learning with self-distillation for weakly-supervised audio-visual violence detection," in *Proc. 30th ACM Int. Conf. Multimedia*, Oct. 2022, pp. 6278–6287.
- [62] Z. Liu, Y. Nie, C. Long, Q. Zhang, and G. Li, "A hybrid video anomaly detection framework via memory-augmented flow reconstruction and flow-guided frame prediction," in *Proc. IEEE/CVF Int. Conf. Comput. Vis. (ICCV)*, Oct. 2021, pp. 13 568–13 577.
- [63] Z. Yang, P. Wu, J. Liu, and X. Liu, "Dynamic local aggregation network with adaptive clusterer for anomaly detection," in *Proc. Eur. Conf. Comput. Vis. (ECCV)*, 2022, pp. 404–421.
- [64] M. Z. Zaheer, A. Mahmood, M. Astrid, and S.-I. Lee, "Claws: Clustering assisted weakly supervised learning with normalcy suppression for anomalous event detection," in *Proc. Eur. Conf. Comput. Vis. (ECCV)*, 2020, pp. 358–376.
- [65] Z. Qing, H. Su, W. Gan, D. Wang, W. Wu, X. Wang, Y. Qiao, J. Yan, C. Gao, and N. Sang, "Temporal context aggregation network for temporal action proposal refinement," in *IEEE/CVF Conf. Comput. Vis. Pattern Recognit. (CVPR)*, Jun. 2021, pp. 485–494.